

## MIT Open Access Articles

*Partitioning of a wide bubbling fluidized bed with vertical internals to improve local mixing and bed material circulation*

The MIT Faculty has made this article openly available. **Please share** how this access benefits you. Your story matters.

**Citation:** Soria-Verdugo, Antonio, Cano-Pleite, Eduardo, Panahi, Aidin and Ghoniem, Ahmed F. 2022. "Partitioning of a wide bubbling fluidized bed with vertical internals to improve local mixing and bed material circulation." Powder Technology, 408.

**As Published:** 10.1016/j.powtec.2022.117771

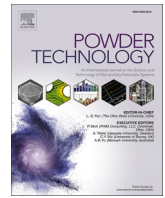
**Publisher:** Elsevier BV

**Persistent URL:** <https://hdl.handle.net/1721.1/152410>

**Version:** Final published version: final published article, as it appeared in a journal, conference proceedings, or other formally published context

**Terms of use:** Creative Commons Attribution Noncommercial No Derivatives 4.0 International





# Partitioning of a wide bubbling fluidized bed with vertical internals to improve local mixing and bed material circulation

Antonio Soria-Verdugo<sup>a,b,\*</sup>, Eduardo Cano-Pleite<sup>a</sup>, Aidin Panahi<sup>b</sup>, Ahmed F. Ghoniem<sup>b</sup>

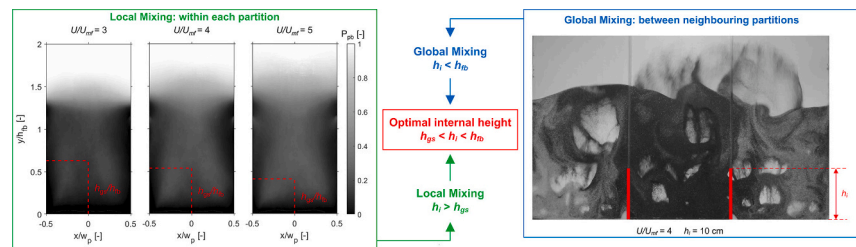
<sup>a</sup> Carlos III University of Madrid (Spain), Thermal and Fluids Engineering Department, Avda. de la Universidad 30, Leganés, 28911, Madrid, Spain

<sup>b</sup> Massachusetts Institute of Technology, Department of Mechanical Engineering, 77 Massachusetts Ave, Rm 3-344, 02139 Cambridge, MA, USA

## HIGHLIGHTS

- Pseudo-2D bed was used to characterize the effect of vertical partitions on mixing.
- Solids with different colors were used to evaluate local and global mixing.
- A model is developed to determine the exchange efficiency between partitions.
- Vortex pair structures appear with internals above the gulf-stream height.
- Vortex structures improve local mixing, global mixing remaining nearly unaffected.

## GRAPHICAL ABSTRACT



## ARTICLE INFO

### Keywords:

Bubbling fluidized bed  
Global mixing  
Local mixing  
Vertical internals

## ABSTRACT

Industrial scale fluidized bed reactors are characterized by limited mixing rates, either local or global, especially when using low-pressure drop gas distributors to reduce operational costs. In this work, partitioning of wide beds using vertical internals is proposed as an effective technique to improve local mixing in large reactors, i.e., mixing in specific zones of the bed. The effect of the vertical internals height on local solids mixing within partitions was experimentally evaluated in a pseudo-2D bed by analyzing the velocity and flow structure of the solids and the circulation time within individual partitions. In the presence of internals, global mixing, i.e., mixing between neighboring partitions and across the entire reactor, may be reduced as vertical internals compartmentalize the bed. Thus, the effect of the internals height on global mixing was also quantified while using bed materials with the same properties, but differing in color, in the different partitions, and analyzing the time evolution of the concentration of solids. Furthermore, the effect of internals on bubbles was also evaluated for different internal heights. It was found that internals with a height between the gulf-stream height and the fixed bed height promote the appearance of vortex pair structures in each partition of the wide bed. These structures substantially improve local mixing within each partition, while global mixing between partitions is practically unaffected by the presence of these short internals.

## 1. Introduction

Fluidized bed (FB) reactors are widely used in industry to convert

*Abbreviations:* BFB, Bubbling Fluidized Bed; CDF, Cumulative Density Function; DIA, Digital Image Analysis; FB, Fluidized Bed; PIV, Particle Image Velocimetry.  
\* Corresponding author at: Carlos III University of Madrid (Spain), Thermal and Fluids Engineering Department, Avda. de la Universidad 30, Leganés, 28911 Madrid, Spain.

E-mail address: [asoria@ing.uc3m.es](mailto:asoria@ing.uc3m.es) (A. Soria-Verdugo).

<https://doi.org/10.1016/j.powtec.2022.117771>

Received 13 January 2022; Received in revised form 3 June 2022; Accepted 21 July 2022

Available online 25 July 2022

0032-5910/© 2022 The Authors. Published by Elsevier B.V. This is an open access article under the CC BY-NC-ND license (<http://creativecommons.org/licenses/by-nc-nd/4.0/>).

Nomenclature			
$A_0$	Bed cross section per hole of the distributed plate distributor [m <sup>2</sup> ]	$t_m$	Mixing time [s]
$C_0$	Initial concentration of the solids in each partition [–]	$t_b$	Bed thickness [m]
$C_{av}$	Average concentration of the solids in each partition [–]	$t_c$	Average circulation time [s]
$C_i$	Concentration of solids in each partition [–]	$U$	Gas velocity [m/s]
$d_b$	Bubble diameter [m]	$U_b$	Bubble velocity [m/s]
$d_p$	Average size of the bed material particles [m]	$U_{mf}$	Minimum fluidization velocity [m/s]
$f_w$	Wake fraction of bubbles [–]	$V_{dp}$	Volume of dense phase in the bed [m <sup>3</sup> ]
$g$	Gravity acceleration [m/s <sup>2</sup> ]	$v_s$	Solids velocity [m/s]
$H$	Reactor vessel height [m]	$v_s^+$	Solids velocity in the upwards direction [m/s]
$h_b$	Bed height [m]	$v_s^-$	Solids velocity in the downwards direction [m/s]
$h_{fb}$	Fixed bed height [m]	$v_{sm}$	Maximum solids velocity [m/s]
$h_{gs}$	Gulf-stream height [m]	$W$	Bed width [m]
$h_i$	Internals height [m]	$w_p$	Partition width [m]
$h_{max}$	Maximum bed height [m]	$x$	Horizontal coordinate [m]
$h_{mf}$	Bed height at minimum fluidization [m]	$y$	Vertical coordinate [m]
$\dot{m}_{1-2}$	Net solids mass transfer rate between neighboring partitions [kg/s]	<b>Greek letters</b>	
$n_b$	Number of bubbles in a specific region of the bed [–]	$\delta_b$	Bubble fraction in the bed [–]
$N_m$	Number of times the bubbles should rise the solids to attain mixing [–]	$\Delta V$	Proportion of solids volume displaced by bubbles [–]
$N_{par}$	Number of partitions in the bed [–]	$\varepsilon$	Porosity of the dense phase [–]
$P_b$	Proportion of bubbles in a specific region of the bed [–]	$\varepsilon_{mf}$	Void fraction at minimum fluidization [–]
$P_{pb}$	Bubble presence probability [–]	$\eta_e$	Exchange efficiency [–]
$P_{hb}$	Probability of the bed height [–]	$\pi_c$	Dimensionless circulation time of the bed material [–]
$Q_{vis}$	Visible bubble flow [m <sup>3</sup> /s]	$\rho_s$	Density of the solid particles [kg/m <sup>3</sup> ]
$t$	Time [s]	$\sigma_{hb}$	Standard deviation of the bed height [m]
		$\tau_m$	Dimensionless form of the mixing time [–]
		$\psi$	Fraction of the excess gas velocity corresponding to visible bubble flow [–]
		$\phi$	Dimensionless form of the bed height [–]

solid fuels, such as coal or biomass and even low-rank fuels like wastes, urban solid residues or sewage sludge, into useful products. These reactors are endowed with favorable characteristics that include rapid mixing, homogeneous temperature, high thermal inertia, and elevated convection coefficients. However, mixing in wider fluidized beds typical of industrial scale reactors, either locally, i.e., in a specific zone of the reactor, or globally, that is, across the entire bed, may be limited, especially in units with low pressure drop gas distributors [26]. Poor mixing may lead to operational problems such as the generation of hot or cold spots or the formation of agglomerates, which reduces the fluidization quality and could even result in partial or total defluidization of the bed [14,30].

Heat and mass transfer in FB reactors is largely driven by solids mixing [6]. It is generally known that the mixing of bed materials is induced by the rise of bubbles [32], which transport solid particles upwards in their wake from the bottom of the bed to its surface [9]. In contrast, lateral mixing of solids occurs mainly by the coalescence and eruption of bubbles, besides the solid particles flows in the emulsion phase. As a consequence, axial mixing of the bed material is much faster than lateral mixing due to the vertical motion of bubbles [17,33]. The reduced mixing rate in the lateral direction is a limiting factor specially for industrial scale reactors [24,29]. This limitation is typically overcome through the design of optimal feeding ports that improve the distribution of fuel particles across the entire bed cross-section [11]. While fuel axial mixing has some impact on the heat and mass transfer between the fuel particles and the bed [25], poor lateral fuel mixing may induce high concentration of volatile matter and char close to the fuel feeding ports [13]. This could result in undesired temperature profiles [39] and increased pollutant emissions [22], especially when converting high-volatile fuels such as biomass. Therefore, understanding mixing mechanisms of both bed material and fuel particles in bubbling fluidized beds is critical to guaranteeing the proper operation of the reactor.

Measuring and predicting solids mixing rates in bubbling fluidized

beds (BFB) is a complex task due to their complex flow structure [5,10]. Several experimental techniques have been successfully applied to characterize solids mixing using, e.g., radioactive tracers, including <sup>198</sup>Au [28] or <sup>18</sup>F [23]. Recently, Martinez et al. [26] measured the temperature field of the bed surface to infer the mixing of solids in a lab-scale version of their gasifier. Pseudo-2D beds are also extensively used for the same purpose since they allow optical access to the bed through their transparent walls. In these studies, analyses can be focused on some tracer particles [31] or on determining the mixing of all particles using different colors for the solids forming the bed [16,34]. Recently, Vandewalle et al. [38] found, based on experimental measurements in a pseudo-2D bed and on numerical simulations, that mixing can be improved by gas pulsation and partial compartmentalization of the bed. The experimental evidence of solid mixing collected in pseudo-2D beds can be useful to qualitatively describe the mixing process, considering the 2D patterns of solids flow. In addition, the general trends observed in pseudo-2D beds can be extrapolated with caution to 3D units. However, special attention shall be paid when extrapolating the quantitative results attained in pseudo-2D beds to 3D reactors, as specific characteristic of 3D beds, such as toroidal solids flow patterns, should be considered. The detailed experimental information obtained from measurements in pseudo-2D beds can be used to validate complex CFD models of the mixing process that can be latter adapted to 3D units. We emphasize that previous studies have demonstrated that even for nominally “2D” beds, the CFD approach should be 3D since 2D simulations do not resolve the gas and solids flow in the third direction and the boundary conditions on the front and rear walls, which are critical parameters affecting the fluid dynamics of the bed [4].

In this work, a wide pseudo-2D bed was used to characterize the effect of vertical internals on the mixing of bed material. Vertical internals were selected since they are subjected to lower rates of erosion and abrasion and allow the operation of different partitions of the bed as independent entities if the gas supplied through the distributor can be

controlled in each partition. In this study, local mixing is defined as mixing of bed material within each partition, whereas global mixing is defined as mixing of the solids across the entire bed. The partitioning of the bed is a novel concept that could be applied to improve local mixing, potentially without hampering global mixing in wide beds. Solids with identical properties but different in color were used in the central and lateral partitions of the pseudo-2D bed. The experimental setup and measurement technique are described in Section 2. The bed was video recorded through the transparent frontal wall, to determine the mixing time based on the concentration of solid in each partition. Moreover, the approach enables characterizing the solids velocity and the bubble characteristics. Experimental data are analyzed in Section 3. The effect of internals on mixing, both locally and globally, were quantified by varying the height of the internals. A model is developed to relate the exchange efficiency between partitions and other characteristic performance parameters, and it was used along with experimental data to determine the impact of internals on global mixing. Conclusions are summarized in Section 4.

## 2. Experimental setup

### 2.1. Experimental facility

The effect of the internals height,  $h_i$ , on the mixing of bed material in a partitioned BFB was examined using a pseudo-2D lab-scale facility. The bed vessel had a total height of  $H = 60$  cm, its total width was  $W = 60$  cm, and the bed thickness was  $t_b = 1$  cm. The front wall was transparent to allow optical access of a video camera to the bed, whereas the rear wall was semi-transparent. The bed was video recorded at 30 fps through the transparent front wall by a regular video camera. The bed was illuminated through the semi-transparent rear wall by two spotlights symmetrically located behind the bed. This arrangement allowed illuminating the bed and distinguishing the bubbles, while avoiding the saturation of the images by direct illumination of the camera through the bubbles. An additional spotlight, located above the camera, was used to illuminate the front of the bed to avoid undesired reflections. A schematic of the experimental setup is shown in Fig. 1.

A small vertical track of 5 mm in width and 5 mm in depth was milled in both the front and rear walls of the bed to place the internals that partitioned the bed into three zones of width  $w_p = 20$  cm. The volume of each vertical track guide corresponds to only 0.4% of the total volume of the bed, thus, their effect on mixing and the mixing time is slight. In fact, a comparison between the mixing measurements with no internals in a

bed with flat front and rear internal surface walls (i.e., no vertical track) resulted in similar values to those obtained in the bed with the vertical track guides. The plenum was also divided to independently control the gas velocity into each partition, contributing to attaining a homogeneous gas distribution along the bed width without the requirement of a high pressure drop distributor. Air at room temperature was used as the fluidizing agent, using a digital flowmeter PFM711S-02-E from SMC to measure the gas velocity. The distributor was a perforated plate with a total of 57 holes of 1 mm in diameter, i.e., 19 holes in each of the 3 partitions. The holes were separated by 1 cm except those corresponding to 2 different partitions that were separated by 2 cm. Thus, holes were drilled each 1 cm except those 2 coinciding where the internals are located, i.e., in the track where the internals were placed, which were not drilled. A mesh was also used to prevent the bed material from falling into the plenum chamber. The distributor was designed to provide a pressure drop of around 30% of the bed pressure drop at minimum fluidization velocity to guarantee proper gas distribution, as suggested by Karri and Werther [19]. The relation of the distributor pressure drop,  $\Delta p$ , and the superficial gas velocity,  $u$ , obtained by fitting of experimental measurements is  $\Delta p [\text{Pa}] = 8.1 \cdot 10^4 (u [\text{m/s}])^2$ .

During the tests, the same gas velocity was used for the three partitions, with values of  $U/U_{mf} = 3, 4$  and 5, and the bed was video recorded for 10 min to analyze the mixing of bed material. For each gas velocity, the height of the intervals  $h_i$  was varied from 0 to 35 cm in 5 cm increment, resulting in a total of 24 different experiments.

### 2.2. Bed material

The bed material was Ballotini glass beads, with a diameter range between 200 and 300  $\mu\text{m}$ , the density being 2500  $\text{kg/m}^3$ , corresponding to Geldart's type B particles [12]. The measured minimum fluidization velocity was  $U_{mf} = 8.3$  cm/s. Particles with the same properties but different color (black and white) were used in the different partitions to characterize mixing. A total of 1650 g of particles were used in each test, with 550 g of white particles introduced in the lateral partitions and 550 g of black particles placed in the central partition, corresponding to a fixed bed height of  $h_{fb} = 18.0$  cm in all partitions. As expected, the fluidized bed height  $h_b$ , given in the following section, was higher than  $h_{fb}$  because of the gas flow. This is why higher internals, up to  $h_i = 35$  cm, were used to examine the impact of partitioning on bed dynamics and particle mixing.

## 3. Results and discussion

### 3.1. Bed height

The bed height was determined using Digital Image Analysis (DIA) of the videos recorded with no internals and with the entire bed fluidized at the same dimensionless gas velocity of  $U/U_{mf} = 3, 4$ , and 5. A total time of 2 min of operation was analyzed for each gas velocity, corresponding to 3600 images. For each snapshot, the bed height was determined by averaging the vertical position of the free surface across the width. The average bed height was found to follow a normal distribution, with an average  $h_b$  and a standard deviation  $\sigma_{hb}$ . Thus, the maximum average height  $h_{max}$  was taken as  $h_{max} = h_b + 3\sigma_{hb}$ , and the probability of having a bed height above this maximum is less than 0.14%. The characteristic values of the normal distribution of bed heights obtained from DIA of the

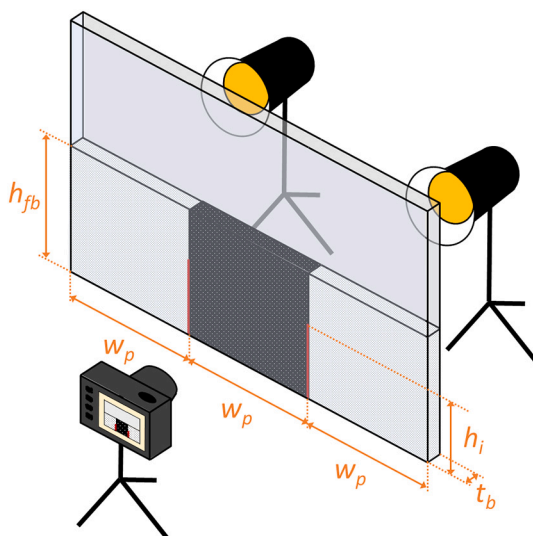


Fig. 1. Schematic of the experimental setup.

Table 1

Characteristic values of the normal distribution of bed heights as a function of the gas velocity for a fixed bed height of  $h_{fb} = 18.0$  cm.

$U/U_{mf} [-]$	$h_b$ [cm]	$\sigma_{hb}$ [cm]	$h_{max}$ [cm]
3	24.3	1.2	27.9
4	26.5	1.7	31.6
5	28.0	2.2	34.6



videos are reported in Table 1.

As expected, the bed height increases with the gas velocity as a consequence of the presence of larger bubbles, which produce higher bed height fluctuation, as manifested by the increasing higher standard deviation.

A rough estimate of the bed height can be predicted using the bubble fraction  $\delta_b$  and the minimum fluidization height, which in this case was very close to the fixed bed height  $h_{mf} \approx h_{fb} = 18.0$  cm, as follows:

$$\frac{h_b}{h_{mf}} = \frac{1}{1 - \delta_b} \quad (1)$$

The bubble fraction in the bed  $\delta_b$  was determined from the correlation proposed by Kunii and Levenspiel [20], neglecting gas throughflow for intermediate bubbles, i.e., when  $U_{mf}/\varepsilon_{mf} < U_b < 5U_{mf}/\varepsilon_{mf}$ , where  $\varepsilon_{mf}$  is the void fraction of the bed at minimum fluidization velocity,  $U_{mf}$  is the minimum fluidization velocity of the bed material,  $U_b$  is the bubbles velocity, and  $U$  is the gas velocity.

$$\delta_b = \frac{U - U_{mf}}{U_b + U_{mf}} \quad (2)$$

The bubble velocity  $U_b$  was calculated by means of the widely known correlation of Davidson and Harrison [8], Eq. (3), for which the bubble diameter  $d_b$  was estimated according to Darton et al. [7], Eq. (4):

$$U_b = U - U_{mf} + 0.711\sqrt{g d_b} \quad (3)$$

$$d_b = 0.54 g^{-0.2} (U - U_{mf})^{0.4} [h_b + 4\sqrt{A_0}]^{0.8} \quad (4)$$

where  $g$  is the gravity acceleration,  $A_0$  is the bed cross section per unit of holes of the perforated plate distributor.

The probability distribution of the bed height is depicted by a colormap in Fig. 2, together with the estimates from Eq. (1), as function of the dimensionless gas velocity. The height of the internals tested in this work is also indicated in the figure by horizontal black dotted lines. The average value of the bed height is in good agreement with the estimated value, Eq. (1), illustrated with a dashed red line in Fig. 2.

### 3.2. Local mixing within a partition

The local mixing within each partition was evaluated based on the flow structure of the solids in that region. The flow structures formed by the solid particles were determined by applying the multigrid Particle Image Velocimetry (PIV) code MATPIV [37] to the video images. The solids velocity field obtained from instantaneous images was averaged according to Laverman et al. [21]. The solids velocity in this 2D bed is known to be affected by the wall [15], and hence, quantitative results

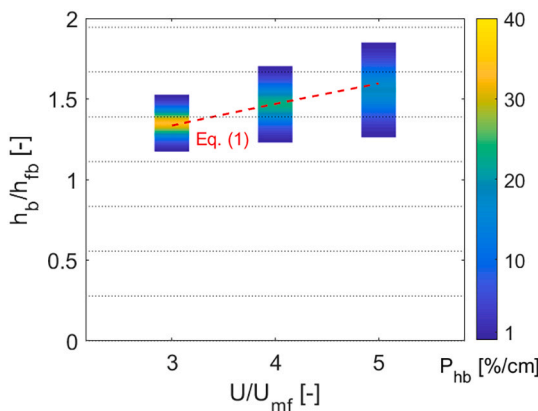


Fig. 2. Bed height probability distribution for each gas velocity. The horizontal black dotted lines represent the height of internals tested in dimensionless form  $h_i/h_{fb}$ .

obtained from this technique cannot be directly extrapolated to 3D beds. However, relevant qualitative results can still be extracted. The solids average velocity in the central partition is depicted in Fig. 3 for all tested dimensionless gas velocities.

The normalized magnitude of solids velocity, using the maximum value measured for all the internal heights of a specific gas velocity, i.e.,  $v_s/v_{sm}$ , is represented in Fig. 3 in the form of a color map, with the magnitude and direction shown by the arrows. A clear effect of the height of internals on both the magnitude of velocity and the structure of the solids flow can be observed. The upwards velocity of solids in the central partition is more uniform across the bed width with no internals. Increasing the height of internals slows down the velocity near the internals and accelerates the solids at the center of the partition. This acceleration is more significant at higher gas velocities. At  $U/U_{mf} = 3$  the maximum solids velocity is similar for all the internals. In all cases, the solids flow pattern evolves from an almost uniform distribution with no internals, to a well-defined vortex pair structure typical of narrow beds, that is, beds with a height to width ratio close to 1. This vortex pair structure obtained for all the gas velocities for higher internals heights,  $h_i > 20$  cm, is similar to that obtained for  $h_i = 20$  cm, hence, they were not included in Fig. 3. The vortex pair structure is associated with a preferential path for bubbles acting as rising channels for the bed material, and two descending paths for the solids close to the vertical internals [35], in what is known as a recirculation cell [31].

Progressively higher internals promote the formation of two paths of bubbles rising from the sides toward its center where they eventually merge at what is known as the gulf stream [2,27]. The height  $h_{gs}$  of the gulf stream is the height above which the number of bubbles in the lateral sides next to the walls of the bed or partition is smaller than the number of bubbles in the central region of the bed/partition:

$$\forall y \geq h_{gs}, \sum_{\text{centre}} n_b(x, y) \geq \sum_{\text{lateral}} n_b(x, y) \quad (5)$$

where  $n_b$  denotes the number of bubbles. The central region is defined as half the bed/partition surrounding the vertical axis and the lateral regions are the adjacent zones to the central region. The gulf stream height is evaluated for the central partition by dividing the height of the bed into  $\Delta y = 1$  cm bins. Bubbles whose area is smaller than  $1 \text{ cm}^2$  and whose distance to the bottom or lateral walls is smaller than 2.5 cm are discarded to avoid spurious effects. Fig. 4 presents the results for the three gas superficial velocities operated with internals of  $h_i = 20$  cm. The results are presented on a percentage basis so that, in each bin, the figure shows the proportion of bubbles,  $P_b$ , located at the center or the lateral sides of the bed. For all three gas superficial velocities, more bubbles are found in the lateral sides up to a height in which the bubble lateral paths meet and the bubble count in the central region becomes larger than in the laterals. The intersection of the curves shown in Fig. 4 determines the height above which bubbles rise predominantly through the center of the bed, i.e., the gulf-stream height  $h_{gs}$ , and corresponds to  $h_{gs} = 11.3$ , 9.7 and 7.4 cm for dimensionless gas velocities of  $U/U_{mf} = 3$ , 4 and 5, respectively. These results are in good agreement with those previously determined by Bakshi et al. [2] from numerical simulations.

The quantitative values obtained for  $h_{gs}$  are in good agreement with the qualitative observations from the images showing the central compartment of the bed. As an example, Fig. 5 shows the average grayscale maps of the images of the central compartment during 2 min for the three gas superficial velocities and internals of  $h_i = 20$  cm, rescaled between 0 and 1. In the figure, a lighter color indicates a higher probability of finding a bubble. Also included in the figure are the values of  $h_{gs}$ . Note that in Fig. 5, bubbles rise predominantly along the sides of the partition and their paths eventually merge in the central region, forming a single bubble path. The height of this merging point can be visually identified, it clearly decreases when increasing the gas superficial velocity. The estimated values of  $h_{gs}$  provide a good marker of the merging point, that also agrees with the position above which the two

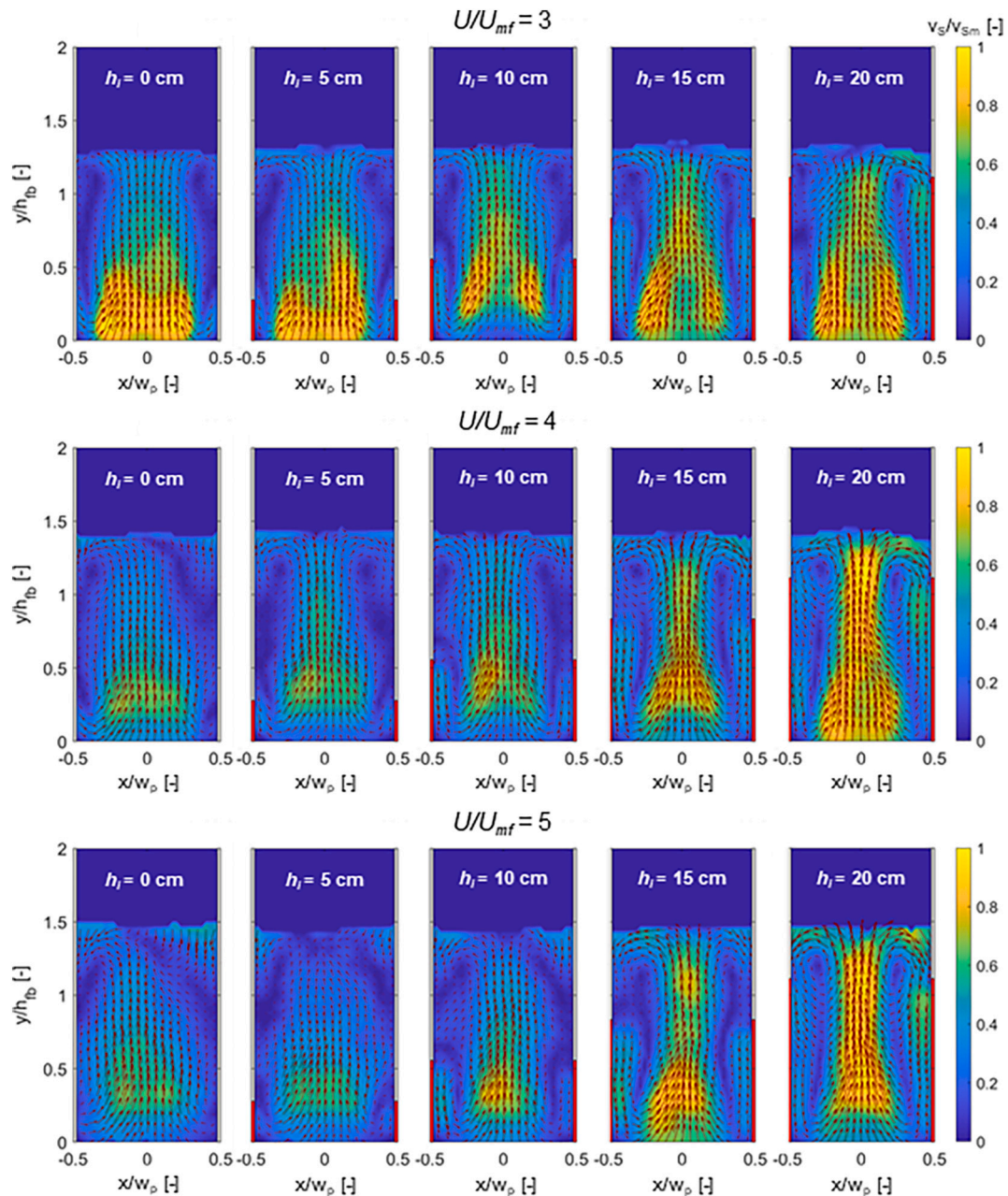


**Fig. 3.** Average velocity field showing the solids motion pattern in the central partition for all gas velocities (internals are represented in red color at both sides of the partition). (For interpretation of the references to color in this figure legend, the reader is referred to the web version of this article.)

lateral bubble paths can be considered as a single path.

From the average velocity of the solids obtained from the multigrid PIV of the recorded images, depicted in Fig. 3, an average circulation time can be obtained for the solids in each partition of the bed. The average circulation time  $t_c$  was calculated from the average solid velocities in the upwards  $v_s^+$  and downwards  $v_s^-$  directions, obtained from the multigrid PIV results, according to Bakshi et al. [2] and Bakshi et al. [3]:

$$t_c = \int_{y_{min}}^{y_{max}} \frac{dy}{v_s^+} + \int_{y_{min}}^{y_{max}} \frac{dy}{v_s^-} \quad (6)$$

The circulation time is proportional to the local mixing time, i.e., the time required to attain a proper mixing in each partition. This time is represented in Fig. 6 for each gas velocity as a function of the height of internals in dimensionless form  $\pi_c$ , normalizing each value with the

circulation time obtained when no internals were present in the bed for each gas velocity. The comparison of the results for different heights of internals was shown in the figure by the dimensionless parameter  $\pi_c$  to avoid the wall effect of the front transparent wall on the average solids velocity obtained from the multigrid PIV measurements. Although only qualitative results for the circulation time can be extracted from the multigrid PIV results of the average solids velocity, the effect of introducing internals can be determined from the dependency of the dimensionless circulation time  $\pi_c$  on  $h_i$ . A significant reduction of the dimensionless circulation time can be observed in Fig. 6 when increasing the height of internals up to 20 cm. A similar decrease of the dimensionless circulation time was obtained for all the gas velocities tested, for internals of  $h_i \leq 15$  cm. However, for a height of internals of  $h_i = 20$  cm the circulation time was similar to that obtained for  $h_i = 15$  cm for a gas velocity of  $U/U_{mf} = 3$ , whereas for  $U/U_{mf} = 4$  and 5, the circulation time still decreased for  $h_i = 20$  cm. This may be caused by the lower bed

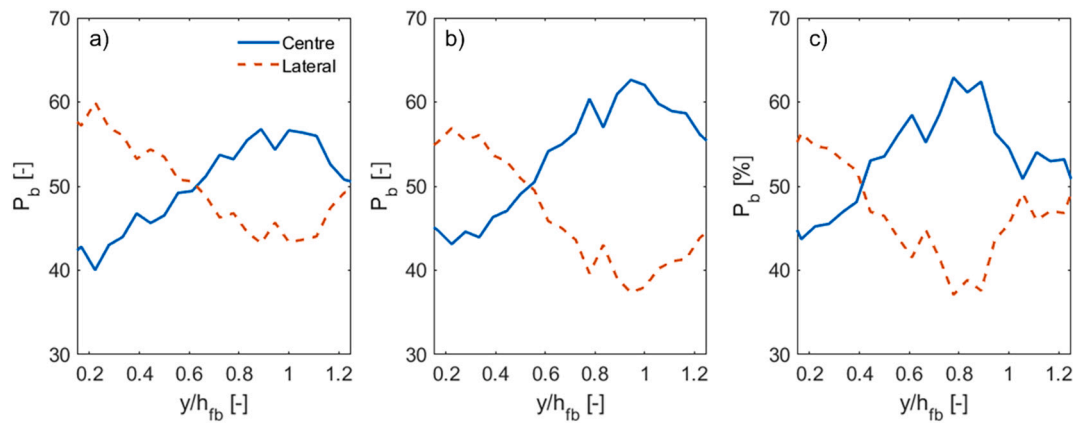


**Fig. 4.** Proportion of bubbles located at the center and lateral sides of the central partition as a function of the height. Bed operated with internals of  $h_i = 20$  cm and a)  $U/U_{mf} = 3$ , b)  $U/U_{mf} = 4$ , c)  $U/U_{mf} = 5$ .

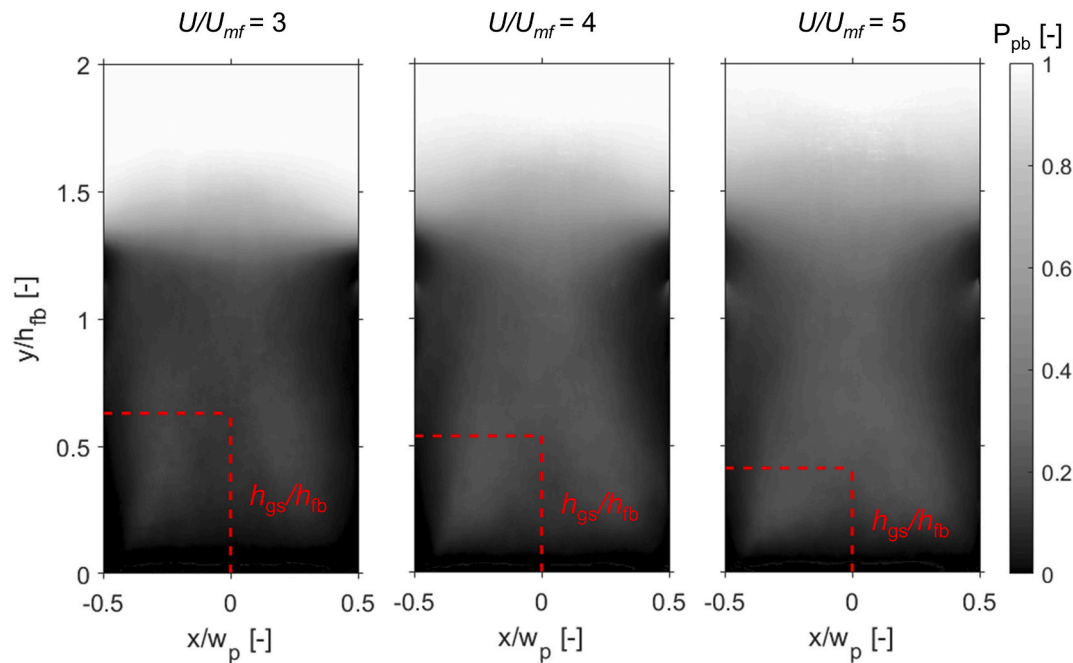


**Fig. 5.** Average grayscale images of the central compartment during 2 min for a height of internals of  $h_i = 20$  cm and different gas superficial velocities rescaled between 0 and 1.  $h_{gs}$  indicates the height above which bubbles are more probably present in the center than at the sides of the bed partition.

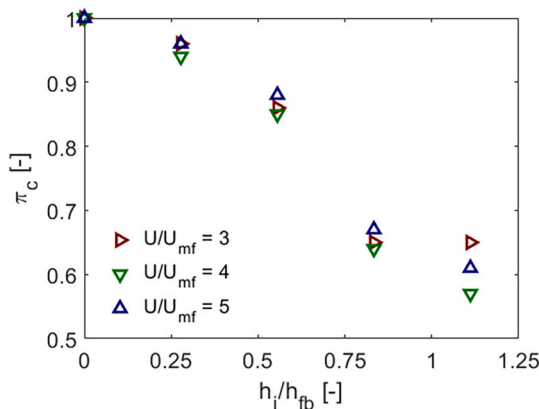


**Fig. 6.** Dimensionless circulation time within each partition of the bed as a function of the height of internals for all gas velocities tested.

height for  $U/U_{mf} = 3$  (Table 1), for which the vortex pair configuration for the solids flow is already attained with internals of  $h_i = 15$  cm. Nonetheless, a reduction of the circulation time of at least 35% can be accomplished using internals of 20 cm compared to fluidizing the bed with no internals for all the gas velocities tested.

The highest reduction of the dimensionless circulation time  $\pi_c$  depicted in Fig. 6 was found for a height of internals between 10 and 15 cm for the three dimensionless gas velocities tested, that is, for a height of internals above the gulf-stream height, which promotes the appearance of vortex pair structures for the solids circulation in the partition. The analysis of the local mixing in each partition concluded that increasing the height of internals above the gulf-stream height promoted the formation of vortex pair structures for the solids flow in each partition, which results in a substantial reduction of the circulation time for the solids, i.e., a significant reduction of the local mixing time within each partition. These vortex pair structures that forms as the height of internals increases is especially relevant for applications where solids circulation should be enhanced, such as coating of bed material. The



presence of internals in a wide fluidized bed promotes the formation of a vortex pair structure, enhancing local solids mixing within the partition [36]. While local mixing in each partition is improved by installing vertical internals to compartmentalize the bed, the appearance of a bubble preferential path at the center of the partition due to bubbles coalescence may contribute to bubble growth in the bed. The presence of larger bubbles would be a drawback in FB reactors. Thus, an analysis of the effect of internals on the bubbles size is addressed in the next section.

### 3.2.1. Effect of internals on the size of bubbles

The effect of the vertical internals on the size of bubbles was also studied. Bubbles with an equivalent diameter  $d_b > 1.5$  cm were detected in all partitions for each gas velocity and for all internals height. The effect of the internals height on bubbles is small for  $h_i > 20$  cm. Thus, the analysis of the effect on bubbles was focused on  $h_i \leq 20$  cm.

The Cumulative Distribution Functions (CDF) of the bubble diameters obtained from applying DIA to the videos are illustrated in Fig. 7 for all  $U/U_{mf}$  and  $h_i$ . For all the internals heights, larger bubbles were detected for higher gas velocities because of the higher excess gas velocity  $U - U_{mf}$ . The effect of the internals on the size of the bubbles is also visible in Fig. 7, where larger bubbles can be observed when increasing the height of the internals used to compartmentalize the bed. This effect is stronger for low gas velocities, for which the rate of coalescence of bubbles is lower. However, for high gas velocities, at which industrial reactors are typically operated, the effect of vertical internals is small. Therefore, partitioning of wide fluidized beds by vertical internals has a minor effect on bubbles size, especially for high gas velocities.

### 3.3. Global mixing across the entire bed

Fluidized bed partitioning by vertical internals substantially improves local mixing within each partition, while showing a minor effect on bubble size. However, it may still significantly reduce global mixing across the entire bed width. Thus, the effect of internals height on global mixing is analyzed in this section.

The global mixing experiments were performed fluidizing the three partitions with the same dimensionless gas velocity of  $U/U_{mf} = 3, 4$ , and 5 with all the possible vertical internal heights. Initially, the central partition was filled with black particles, whereas the lateral partitions were filled with white particles. The beginning of the test is taken as the moment when fluidizing air arrives at the plenum chamber of the bed, while the particles are still unfluidized. Therefore, the tests include a startup transient from the non-fluidized initial condition to the steady state. Considering the average bubble velocity, given by Eq. (3), and the maximum average bed height, reported in Table 1 for each gas velocity, the residence time of bubbles is around 0.35 s for  $U/U_{mf} = 3, 4$  and 5. Therefore, the startup transient to reach steady state can be considered

negligible compared to the global mixing time between neighboring partitions. Once bubbles appear in the bed, the white and black solids located initially in different partitions mix as time progresses. Figs. 8, 9 and 10 show snapshots of the bed surface for time intervals of 5 s, fluidizing the bed with a gas velocity of  $U/U_{mf} = 4$  using internals of  $h_i = 0, 10$ , and 20 cm, respectively. The effect of internals on the flow can be observed by comparing Figs. 8, 9 and 10. Fig. 8 shows that bubbles are more homogeneously distributed across the bed width without internals. In contrast, fluidizing with higher internals like in Fig. 10 results in a more structured bed, with one bubble per partition close to the bed free surface. For the intermediate situation, i.e., for intermediate internals of  $h_i = 10$  cm, bubbles coming from neighboring partitions can still coalesce over the internals, as shown in Fig. 9 for  $t = 35$  s.

The time evolution of the average concentration of solids in each partition was determined using DIA by means of the time evolution of the average gray level in each partition. The mixing time  $t_m$  was estimated by the time when the average concentration of all partitions equilibrates and remains steady. The average concentrations in each partition obtained from the grayscale images are depicted in Fig. 11 for a gas velocity of  $U/U_{mf} = 4$  using internals of  $h_i = 0, 10$  and 20 cm, i.e., for the same cases shown in Figs. 8–10. In all cases, the time evolution of the average concentration in each partition shows oscillations due to the effect of passing bubbles. The average concentration in the side partitions decreases while remaining similar to each other, confirming the symmetry of the pseudo-2D bed. In contrast, the average concentration in the central partition increases as the black solids are dispersed to the side partitions. The asymptotic value attained by the average concentration in the lateral partitions are similar, while that in the central partition reaches a slightly higher value. The mixing time was determined as the time when the two asymptotic values intersect. To avoid any effect of the fluctuations caused by the passing bubbles, the average concentrations were smoothed using a moving average filter of 10 points applied 300 times to obtain the average evolution of the concentration in each partition. Using the filtered signal resulted in reliable and repetitive values of the mixing time, obtaining deviations below 10% between replicates of the same mixing tests. The mixing time obtained from the filtered signal coincides with that obtained from the first derivative of the filtered curve. In the case of  $U/U_{mf} = 4$  using internals of  $h_i = 0$  cm, the mixing time, represented with an arrow in Fig. 11 a), was 28.7 s, whereas for  $h_i = 10$  and 20 cm the mixing time was 32.0 and 34.5 s, respectively, illustrated in Fig. 11 b) and c) with arrows.

The mixing time  $t_m$  for each height of internals  $h_i$  and gas velocity  $U/U_{mf}$  are plotted in Fig. 12. Shorter mixing times were obtained for higher gas velocities for all  $h_i$  as a result of a more vigorous fluidization induced by larger bubbles. The presence of internals significantly affect the global mixing time, especially for internals height above  $h_i > 20$  cm, i.e., above the fixed bed height  $h_b = 18$  cm. On the other hand, for  $h_i \leq$

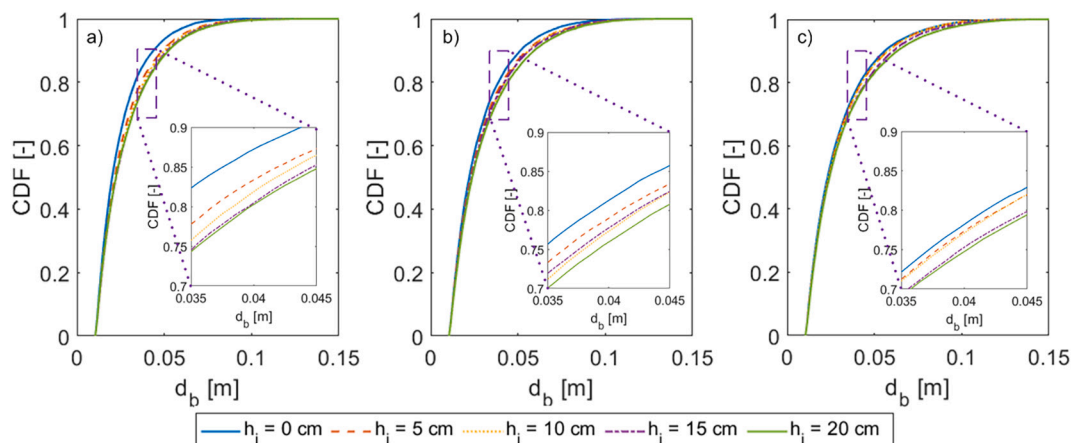


Fig. 7. Cumulative Distribution Function (CDF) of the bubble diameters for gas velocities of a)  $U/U_{mf} = 3$ , b)  $U/U_{mf} = 4$ , c)  $U/U_{mf} = 5$ .

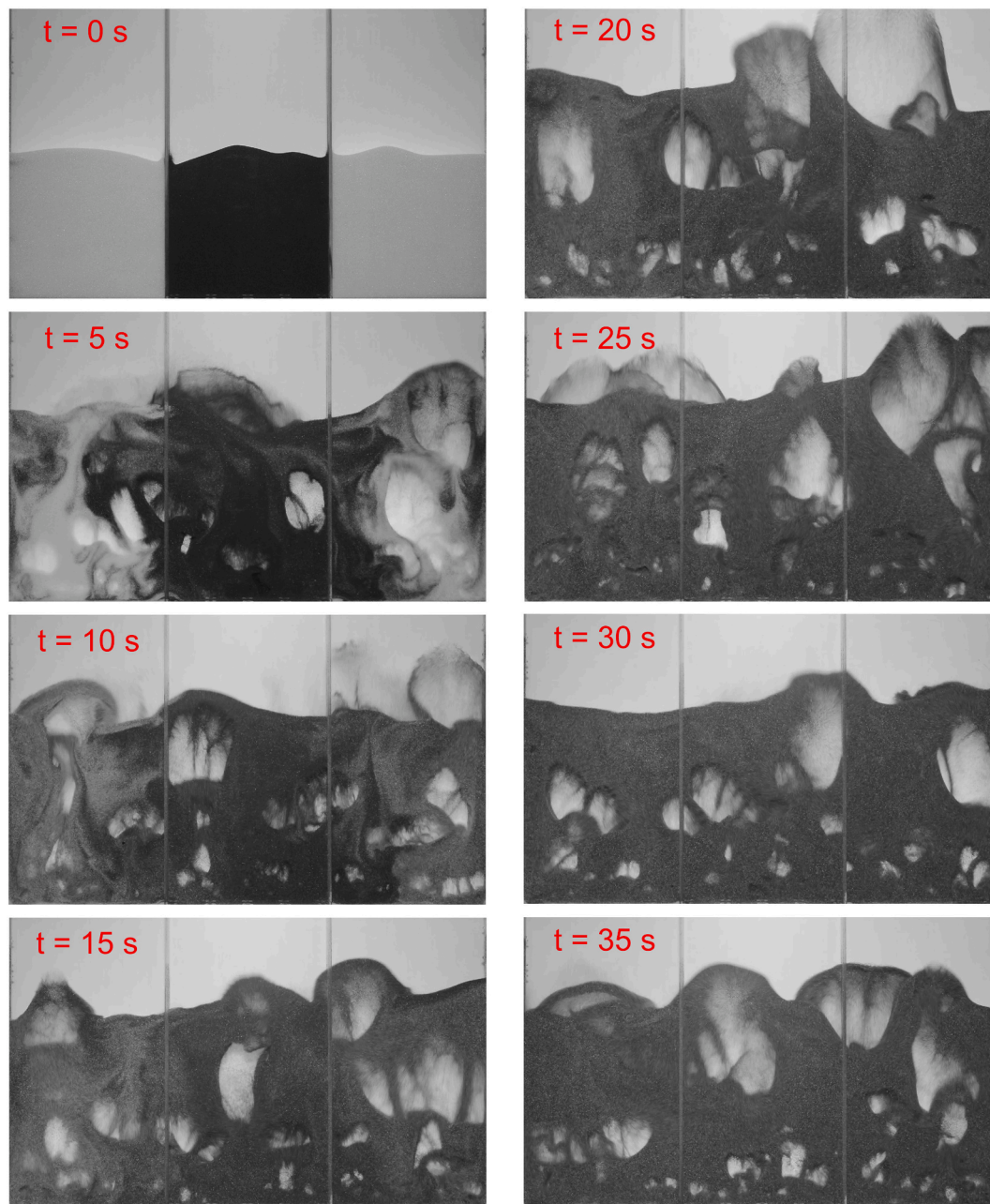


Fig. 8. Snapshots of the bed surface during global mixing test for a gas velocity of  $U/U_{mf} = 4$  using no internals,  $h_i = 0$  cm.

20 cm, the mixing time increases slightly with the height of internals for all the gas velocities tested. In contrast, a sharp increase of the mixing time can be observed for taller internals. For instance, for  $U/U_{mf} = 3$  increasing the internals height from 20 to 25 cm raised the mixing time by one order of magnitude, and for  $h_i = 30$  cm no mixing was attained after the experiment time, i.e., 10 min, for this gas velocity, which is indicated in Fig. 12 by a vertical red arrow at  $h_i = 30$  cm. For a gas velocity of  $U/U_{mf} = 4$ , the increase of internals height from 20 to 25 cm raised the mixing time by roughly 100%, ending the experiment again with the bed not completely mixed after 10 min with internals of 30 cm, shown by a vertical green arrow in Fig. 12. In contrast, the sudden increase of the mixing time for  $U/U_{mf} = 5$  occurred when increasing the height of internals from 25 to 30 cm, for which the mixing time augmented approximately by 500%. For the highest gas velocity tested, mixing was undetected at the end of the experiment for  $h_i = 35$  cm, specified by a vertical blue arrow in Fig. 12. The different height of internals at which the sharp increase of the mixing time occurs for each

gas velocity can be attributed to the different average bed height and deviation (Table 1).

Dimensionless representation was applied to the mixing time as a function of the intervals height. The dimensionless height of internals  $\phi$  is defined as the maximum height of the bed above the internals, calculated as the maximum bed height minus the internal height, i.e.,  $h_{max} - h_i$ , over the maximum bed height (Table 1). Thus,  $\phi$  ranges between 0 when internals equal the maximum bed height, and 1 without internals. Negative values of  $\phi$  could be obtained for  $h_i > h_{max}$ , however, these negative values will not be considered since they preclude a complete mixing of the bed material.

$$\phi = \frac{h_{max} - h_i}{h_{max}} \quad (7)$$

The normalized mixing time  $N_m$  was defined as the ratio of the mixing time and the time required by bubbles to move all the solids in the bed. The latter is the volume of dense phase  $V_{dp}$  over the volumetric



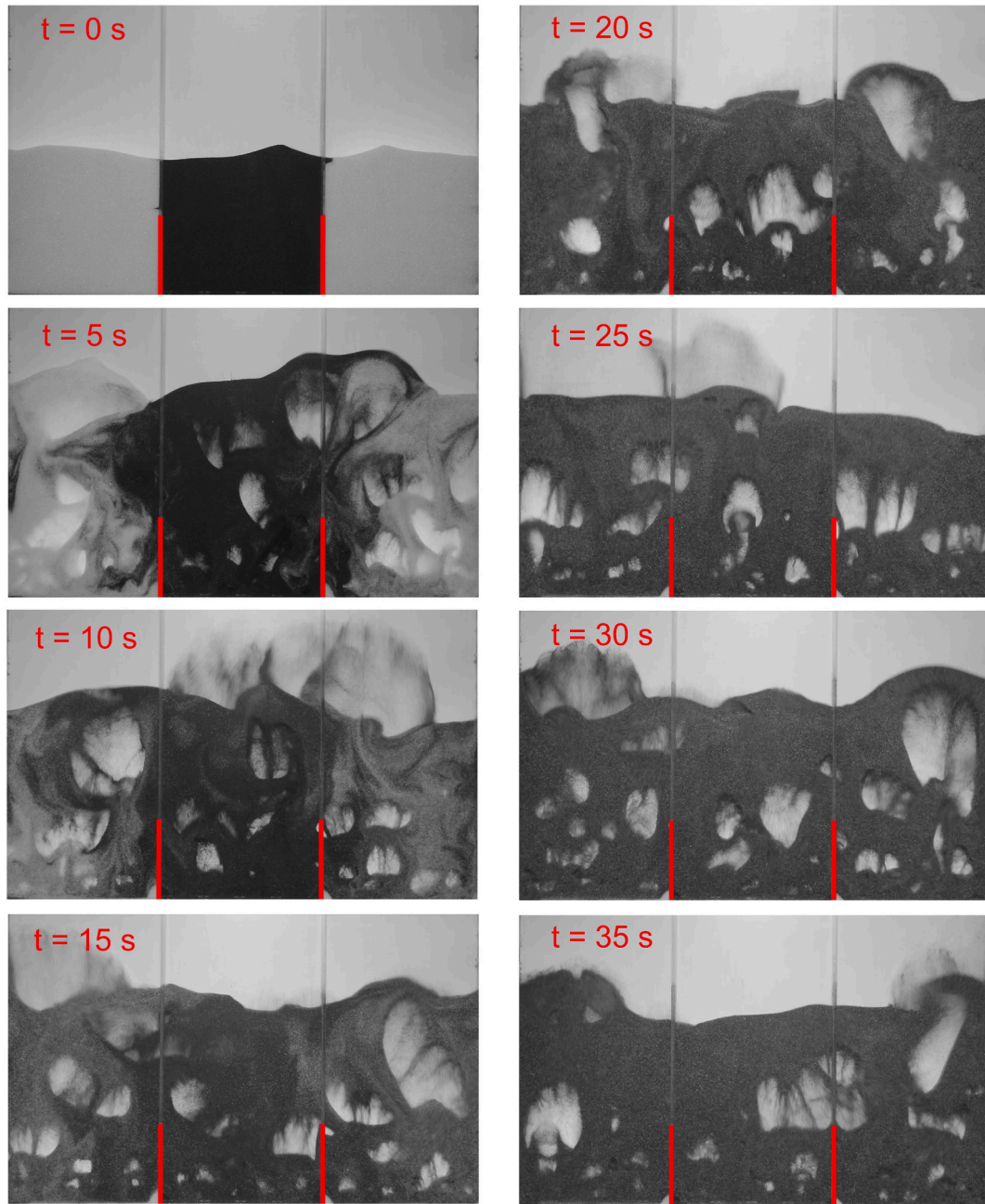


**Fig. 9.** Snapshots of the bed surface during global mixing test for a gas velocity of  $U/U_{mf} = 4$  using internals of  $h_i = 10$  cm, represented by red lines. (For interpretation of the references to color in this figure legend, the reader is referred to the web version of this article.)

flowrate of solids displaced by bubbles, which was calculated as the visible bubble flow  $Q_{vis}$  times the wake fraction of bubbles  $f_w$ . Therefore,  $N_m$  is the number of times the bubbles need in order to move all the solids to reach complete mixing.

$$N_m = \frac{t_m}{V_{dp}/(Q_{vis}f_w)} \quad (8)$$

A wake fraction of  $f_w \approx 0.4$  was used for the glass bead particles of 200–300  $\mu\text{m}$  based on Kunii and Levenspiel [20], while the visible bubble flow  $Q_{vis}$  was estimated for each gas velocity according to Johnsson et al. [18]:

$$\psi = [0.26 + 0.7 \exp(-3.3 d_p)] (0.15 + U - U_{mf})^{-0.33} [h_b + 4\sqrt{A_0}]^{0.4} \quad (9)$$

$$Q_{vis} = \psi (U - U_{mf}) \quad (10)$$

where  $\psi$  is the fraction of the excess gas velocity corresponding to visible bubble flow,  $d_p$  is the average size of the particles, i.e., 250  $\mu\text{m}$  in this case, and  $A_0$  is the bed cross section per holes of the perforated plate distributor.

Fig. 13 shows the values of  $N_m$  as a function of  $\phi$ , for the three values of  $U/U_{mf}$  tested. The normalized experimental measurements depicted in Fig. 12, collapse into a single curve, and the global mixing can be fitted by a rational form:

$$N_m = \frac{1}{\phi - \phi_c} - \frac{1}{1 - \phi_c} + N_{m0} \quad (11)$$

where  $\phi_c$  and  $N_{m0}$  are constants, in this case  $\phi_c = 0.1$  and  $N_{m0} = 15.1$ .  $\phi_c$  corresponds to a critical value of the height of internals for which the number of displacements of the bed material to reach complete mixing

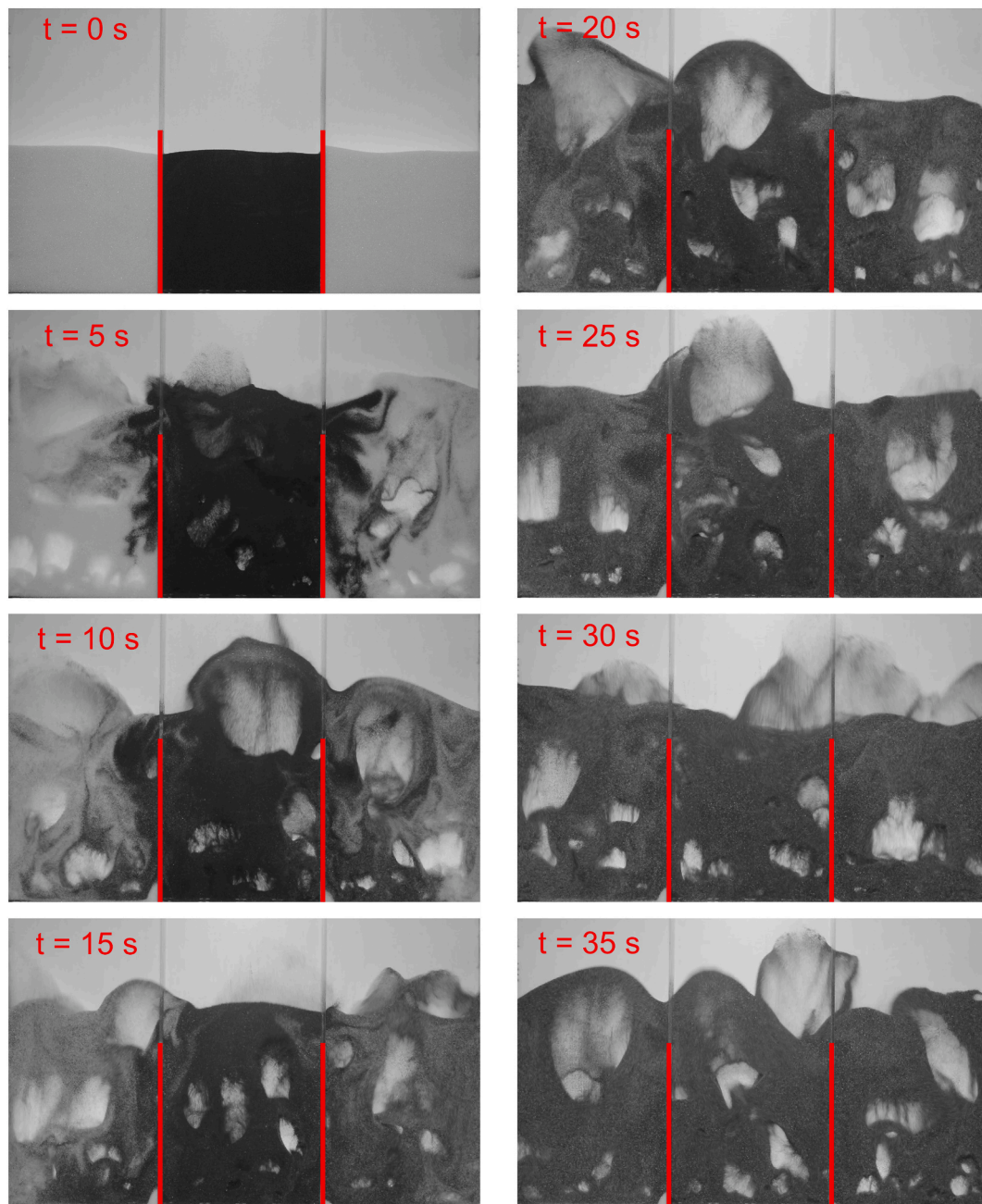


**Fig. 10.** Snapshots of the bed surface during global mixing test for a gas velocity of  $U/U_{mf} = 4$  using internals of  $h_i = 20$  cm, represented by red lines. (For interpretation of the references to color in this figure legend, the reader is referred to the web version of this article.)

tends to infinity, that is, mixing is not attainable for height of internals equal to or above this critical value.  $N_{m0}$  is the number of displacements of the bed material required to attain mixing of the entire bed when no internals are used, i.e., for  $\phi = 1$ . It should be mentioned that  $N_{m0}$  depends on the bed analyzed. Specifically, it depends on the partition width  $w_p$ , with larger values of  $N_{m0}$  expected for wider partitions. The fitting of Eq. (11) is also depicted in Fig. 13 together with the measurements of  $N_m$  and  $\phi$ . A logarithmic scale is used in the x-axis of Fig. 13 to improve visualization of the trend of  $\phi$  close to  $\phi_c$ . As expected, very low values of  $\phi$  largely increase the dimensionless mixing time, its value tending to infinity when  $\phi$  approaches  $\phi_c$ .

### 3.3.1. Efficiency of particles exchange between partitions

For a better understanding of the origin of the values obtained for  $N_m$ , a conceptual experiment is proposed. It consists in considering a bed

with 3 partitions, similar to the one used in the experiments, with equal volume of particles in the three partitions initially, but different color particles in the central and the lateral partitions. Mixing of particles between partitions is modeled as follows. The total mixing time is divided into many steps. In each step, a total of 1% of each partition solids volume is arbitrarily assumed to be displaced by bubbles, i.e.,  $\Delta V = 0.01$ . Part of the displaced solids is exchanged between the central and the lateral partitions according to an assumed exchange efficiency  $\eta_e$ , defined as the percentage of particles raised by bubbles in a specific partition that is displaced to the neighboring partition. Thus, the mutual solids exchange between the central and each of the lateral partitions equal to  $0.5\eta_e\Delta V$ , while the rest of the displaced solids fall back into the same partition. Note that  $0.5\eta_e\Delta V$  is transferred from the central partition to the two the lateral ones, divided equally, whereas only  $0.5\eta_e\Delta V$  in total is transferred from the lateral partitions to the central one due to

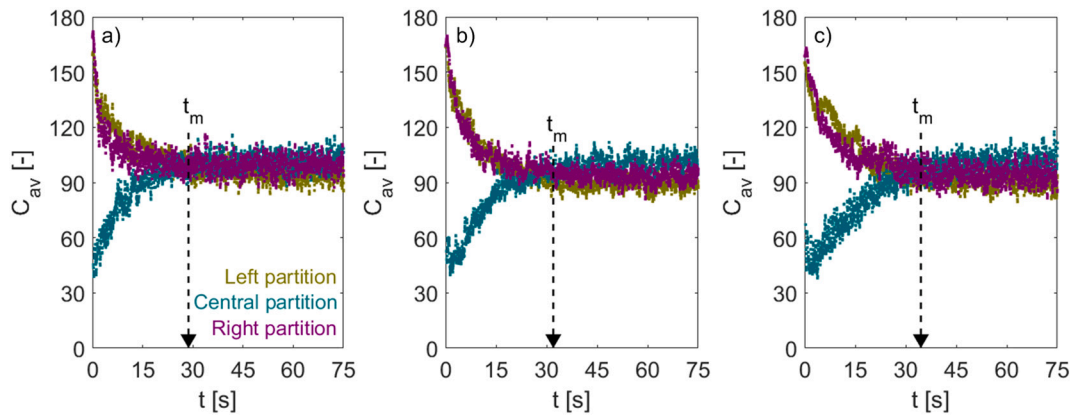


**Fig. 11.** Time evolution of the average concentration measured from the grayscale images of each partition during the global mixing test for a gas velocity of  $U/U_{mf} = 4$  using internals of a)  $h_i = 0$  cm, b)  $h_i = 10$  cm, and c)  $h_i = 20$  cm.

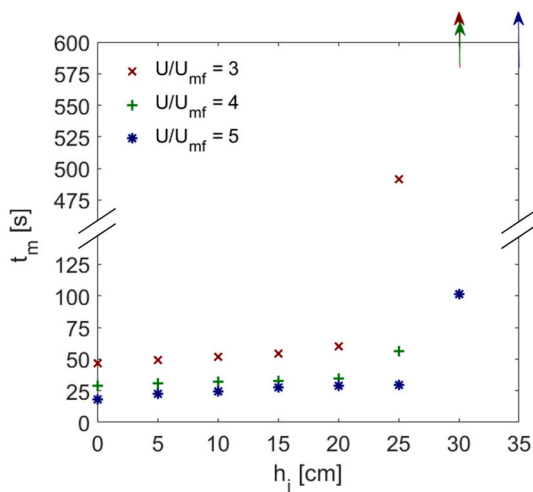


**Fig. 12.** Mixing time  $t_m$  as a function of the internals height  $h_i$  for each gas velocity  $U/U_{mf}$  (color arrows indicate the value of  $h_i$  for which  $t_m$  was higher than the measured time for each case). Notice the broken y-axis.

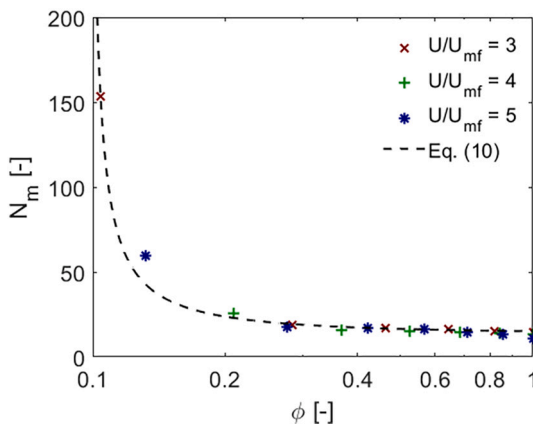


**Fig. 13.** Results of the dimensionless analysis of global mixing for different gas superficial velocities and internal heights.

the presence of the bed walls. A schematic of the conceptual experiment is presented in Fig. 14. The concentration in each partition is then recalculated after each step, and the process is repeated until the bed is completely mixed, that is, when the concentration of each partition is

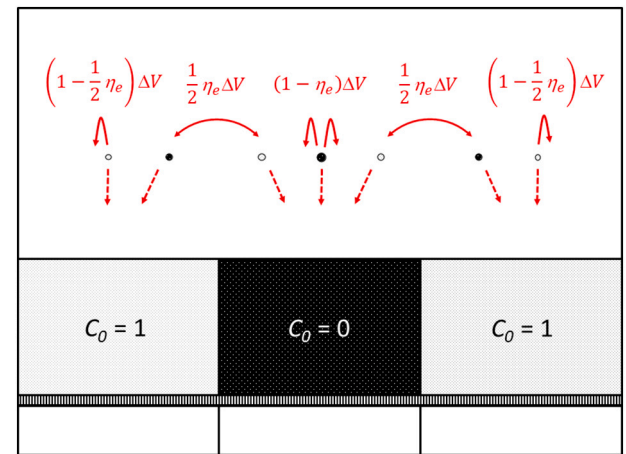


**Fig. 14.** Schematic of the bed used for the conceptual experiment considering the initial concentrations.

equal, with a tolerance of  $10^{-3}$  for the concentrations.

The conceptual experiment was performed to determine the number of times needed for the bubbles to move all the solids in a partition, i.e., the value of  $N_m$ , to reach complete mixing, as a function of the exchange efficiency  $\eta_e$ . The results are depicted in Fig. 15 a). The relation between the parameters follow a rational trend in the form:

$$N_m = \frac{4.6}{\eta_e} \quad (12)$$

Thus, even with an exchange efficiency of 100%,  $\eta_e = 1$ , that is if all the solid particles displaced by bubbles in one partition end up in the neighboring partitions, the solids initially in the original partition should be moved by bubbles 4.6 times to reach a complete mixing across the bed. We should mention that the relation between  $N_m$  and  $\eta_e$  described by Eq. (12) is universal for a bed with 3 partitions, since no geometrical dimensions or any other bed specific parameter were considered in the computation. Clearly, in a real application not all the solids displaced by bubbles in one partition would fall in the neighboring partitions, and then  $\eta_e < 1$ . In fact, for the bed used in our experiments, Eq. (12) can be combined with Eq. (11), which is bed specific, to derive a relation of the exchange efficiency  $\eta_e$  as function of the dimensionless height of internals  $\phi$ . This relation is plotted in Fig. 15 b).

The maximum exchange efficiency  $\eta_e$  for the bed used in the experiments with 3 partitions and  $w_p = 20$  cm with no internals, i.e.,  $\phi = 1$ , is 30.4%. This value is bed dependent and higher values are expected with narrower partitions. The exchange efficiency decreases slightly as  $\phi$  is



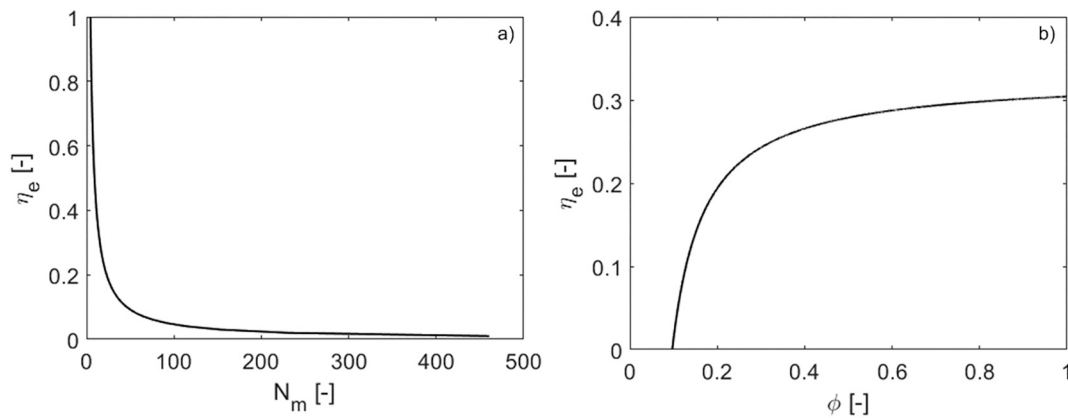


Fig. 15. Relation of the exchange efficiency  $\eta_e$  with a)  $N_m$  and b)  $\phi$ .

reduced when taller internals are used. However, for  $\phi < 0.4$ , a sharp reduction of the exchange efficiency is observed, tending to zero as the internals height approaches the critical value,  $\phi \rightarrow \phi_c$ . Good global mixing can be expected for values for  $\phi > 0.4$ , for which the exchange efficiency remains almost uniform. This condition corresponds to internals with height equal or lower than the fixed bed height for the three gas velocities tested, thus, for good global mixing, the internals height should be  $h_i \leq h_{fb}$ .

In conclusion, a height of vertical internals above the gulf-stream height improves solids mixing within partitions of a wide bed, and keeping the height of internals below the fixed bed height results in a minor effect on the inter-partition mixing. Therefore, the optimal height of vertical internals used to compartmentalize wide fluidized beds is in the range  $h_{gs} \leq h_i \leq h_{fb}$ .

The exchange efficiency between neighboring partitions can be used to estimate the net mass transfer rate of a certain type of particles between adjacent compartments  $\dot{m}_{1-2}$ . The net mass transfer rate depends on the difference of concentration of the selected particles in the partitions,  $C_1 - C_2$ , and on the total mass flow rate of solid particles displaced by bubbles, calculated as a function of the visible bubble flow in each partition  $Q_{vis}/N_{par}$ , the wake fraction of bubbles  $f_w$ , the density of solids  $\rho_s$ , and the dense phase porosity  $\varepsilon$ . Therefore, the net mass transfer rate between neighboring partitions can be determined as follows:

$$\dot{m}_{1-2} = \frac{1}{2} \frac{Q_{vis} f_w \rho_s (1 - \varepsilon) \eta_e}{N_{par}} (C_1 - C_2) \quad (13)$$

In view of Eq. (13), a mass transfer coefficient can be defined, considering the concentrations  $C_i$  defined as number of particles of a certain type divided by the total number of particles, as the parameter multiplying the difference in concentration. This mass transfer coefficient depends on the geometry of the bed, by means of  $N_{par}$  and  $\eta_e$ , the operating conditions, affected by  $Q_{vis}$  and  $f_w$ , and the characteristics of the solids, in terms of  $\rho_s$  and  $\varepsilon$ .

#### 4. Conclusions

The effect of bed partitioning using vertical internals on the mixing of a wide bubbling fluidized bed was studied in this work. Local mixing in each partition was significantly improved by the presence of internals of height above the gulf-stream height, evolving from a nearly uniform solids velocity field when no internals are present, to a vortex pair structure typical of narrow beds, in which the solids move more vigorously. This effect increases remarkably with the height of internals, reducing substantially the circulation time of solids. The effect of the height of internals on bubbles size was also quantified, showing a small increase of the size of bubbles with the internals height, especially for high gas velocities typically used in industrial reactors.

Global mixing between partitions was also analyzed as a function of

the internals height. Global mixing tests were conducted for several gas velocities. Dimensionless representation was applied, resulting in the collapse of all experimental results onto a single curve of the dimensionless mixing time as a function of the dimensionless height of internals. The effect of vertical internals on global mixing was explained in terms of an exchange efficiency of solids between adjacent partitions. The exchange efficiency was practically uniform for internals height up to 20 cm, i.e., around the fixed bed height. Therefore, global mixing is almost not affected by the presence of vertical internals provided that the maximum height of internals is close to that of the fixed bed.

In view of the findings presented in this work, partitioning of wide beds by vertical internals with a height between the gulf-stream and the fixed bed height is recommended, especially in units operating with a low-pressure drop distributor. The presence of these vertical internals improves the solids circulation within each partition, promoting local mixing, whereas global mixing and bubbles' size are nearly not affected by the presence of these vertical internals.

#### Declaration of Competing Interest

The authors declare that they have no known competing financial interests or personal relationships that could have appeared to influence the work reported in this paper.

The authors declare the following financial interests/personal relationships which may be considered as potential competing interests:

#### Acknowledgements

The research that led to this publication was conducted with the support of a US-Spain Fulbright grant co-sponsored by the Spanish Ministry of Universities ("Ministerio de Educación, Cultura y Deporte en el marco del Programa Estatal de Promoción del Talento y su Empleabilidad en I+D+i, Subprograma Estatal de Movilidad, del Plan Estatal de I+D+I"). The authors acknowledge the financial support by the Foundation Seed Fund MIT - Spain "la Caixa". Eduardo Cano-Pleite also acknowledges support from the CONEX-Plus program funded by Universidad Carlos III de Madrid and the European Union's Horizon 2020 program under the Marie Skłodowska-Curie grant agreement No. 801538.

#### References

- [2] A. Bakshi, C. Altantzis, R.B. Bates, A.F. Ghoniem, Study of the effect of reactor scale on fluidization hydrodynamics using fine-grid CFD simulations based on the two-fluid model, *Powder Technol.* 299 (2016) 185–198.
- [3] A. Bakshi, A.F. Ghoniem, C. Altantzis, Mixing dynamics in bubbling fluidized beds, *Aiche* 63 (10) (2017) 4316–4328.
- [4] A. Bakshi, C. Altantzis, A. Bershanska, A.K. Stark, A.F. Ghoniem, On the limitations of 2D CFD for thin-rectangular fluidized bed simulations, *Powder Technol.* 332 (2018) 114–119.

- [5] H.T. Bi, N. Ellis, I.A. Abba, J.R. Grace, A state-of-the-art review of gas–solid turbulent fluidization, *Chem. Eng. Sci.* 55 (2000) 4789–4825.
- [6] G.A. Bokkers, M. van Sint Annaland, J.A.M. Kuipers, Mixing and segregation in a bidisperse gas–solid fluidized bed: a numerical and experimental study, *Powder Technol.* 140 (2004) 176–186.
- [7] R.C. Darton, R. La Nauze, J.F. Davidson, D. Harrison, Bubble growth due to coalescence in fluidized beds, *Trans. Inst. Chem. Eng.* 55 (1977) 274–280.
- [8] J.F. Davidson, D. Harrison, *Fluidised Particles*, Cambridge University Press, Cambridge, 1963.
- [9] I. Eames, M.A. Gilbertson, Mixing and drift in gas–fluidised beds, *Powder Technol.* 154 (2005) 185–193.
- [10] X.F. Fan, Z.F. Yang, D.J. Parker, Impact of solid sizes on flow structure and particle motions in bubbling fluidization, *Powder Technol.* 206 (2011) 132–138.
- [11] L.M. Garcia-Gutierrez, A. Soria-Verdugo, U. Ruiz-Rivas, Optimization of the feeding ports location in a fluidized bed combustor based on Monte Carlo simulations of fuel particles motion, *Fuel* 141 (2015) 82–92.
- [12] D. Geldart, Types of gas fluidization, *Powder Technol.* 7 (1973) 285–292.
- [13] A. Gómez-Barea, B. Leckner, Modeling of biomass gasification in fluidized beds, *Prog. Energy Combust. Sci.* 36 (2010) 444–509.
- [14] J. Gómez-Hernández, D. Serrano, A. Soria-Verdugo, S. Sánchez-Delgado, Agglomeration detection by pressure fluctuation analysis during *Cynara cardunculus* L. gasification in a fluidized bed, *Chem. Eng. J.* 284 (2016) 640–649.
- [15] F. Hernández-Jiménez, S. Sánchez-Delgado, A. Gómez-García, A. Acosta-Iborra, Comparison between two-fluid model simulations and particle image analysis & velocimetry (PIV) results for a two-dimensional gas–solid fluidized bed, *Chem. Eng. Sci.* 66 (17) (2011) 3753–3772.
- [16] F. Hernández-Jiménez, J. Sánchez-Prieto, E. Cano-Pleite, A. Soria-Verdugo, Lateral solids meso-mixing in pseudo-2D fluidized beds by means of TFM simulations, *Powder Technol.* 334 (2018) 183–191.
- [17] O. Ito, R. Kawabe, T. Miyamoto, H. Orita, M. Mizumoto, H. Miyadera, J. Tomuro, N. Hokari, T. Iwase, Direct measurement of particle motion in a large-scale FBC boiler model, *Intern. Conf. Fluidized Bed Combust.* (1999) 217.
- [18] F. Johnsson, S. Andersson, B. Leckner, Expansion of a freely bubbling fluidized bed, *Powder Technol.* 68 (2) (1991) 117–123.
- [19] S.B.R. Karri, J. Werther, Gas distributor and plenum design in fluidized beds, in: W. C. Yang (Ed.), *Handbook of Fluidization and Fluid-Particle Systems*, Marcel Dekker Inc., New York, 2003, pp. 164–179.
- [20] D. Kunii, O. Levenspiel, *Fluidization Engineering*, Butterworth-Heinemann, Stoneham, MA, 1991.
- [21] J.A. Laverman, I. Roghair, M. van Sint Annaland, J.A.M. Kuipers, Investigation into the hydrodynamics of gas–solid fluidized beds using particle image velocimetry coupled with digital image analysis, *Can. J. Chem. Eng.* 86 (2008) 523–535.
- [22] B. Leckner, Fluidized bed combustion: mixing and pollutant limitation, *Progr. Energy Combust. Sci.* 24 (1998) 31–61.
- [23] Y. Li, J. Rong, K. Zhang, X. Fan, Impact of solid and gas flow patterns on solid mixing in bubbling fluidized beds, *Chem. Eng. Res. Des.* 132 (2018) 1037–1053.
- [24] D. Liu, X. Chen, Lateral solids dispersion coefficient in large-scale fluidized beds, *Combust. Flame* 157 (2010) 2116–2124.
- [25] L. Lundberg, P.A. Tchoffor, D. Pallarès, R. Johansson, H. Thunman, K. Davidsson, Influence of surrounding conditions and fuel size on the gasification rate of biomass char in a fluidized bed, *Fuel Process. Technol.* 144 (2016) 323–333.
- [26] Castilla G. Martínez, A. Larsson, L. Lundberg, F. Johnsson, D. Pallarès, A novel experimental method for determining lateral mixing of solids in fluidized beds – quantification of the splash-zone contribution, *Powder Technol.* 370 (2020) 96–103.
- [27] J.M.D. Merry, J.F. Davidson, Gulf-stream circulation in shallow fluidized beds, *Trans. Inst. Chem. Eng.* 51 (1973) 361–368.
- [28] N. Mostoufi, J. Chaouki, Local solid mixing in gas–solid fluidized beds, *Powder Technol.* 114 (2001) 23–31.
- [29] F. Niklasson, H. Thunman, F. Johnsson, B. Leckner, Estimation of solids mixing in a fluidized-bed combustor, *Ind. Eng. Chem. Res.* 41 (2002) 4663–4673.
- [30] J.R. van Ommen, R.J. de Korte, C.M. van den Bleek, Rapid detection of defluidization using the standard deviation of pressure fluctuations, *Chem. Eng. Process.* 43 (2004) 1329–1335.
- [31] D. Pallarès, F. Johnsson, A novel technique for particle tracking in cold 2-dimensional fluidized beds – simulating fuel dispersion, *Chem. Eng. Sci.* 61 (2006) 2710–2720.
- [32] M.J. Rhodes, X.S. Wang, M. Nguyen, P. Stewart, K. Liffman, Study of mixing in gas–fluidized beds using a DEM model, *Chem. Eng. Sci.* 56 (2001) 2859–2866.
- [33] J. Sanchez-Prieto, A. Soria-Verdugo, J.V. Briongos, D. Santana, Stagnant regions estimation in fluidized beds from bed surface observation, *Chem. Eng. J.* 281 (2015) 109–118.
- [34] J. Sánchez-Prieto, F. Fernández-Jiménez, L.M. García-Gutiérrez, A. Soria-Verdugo, Experimental study on the characteristic mixing time of solids and its link with the lateral dispersion coefficient in bubbling fluidized beds, *Chem. Eng. J.* 307 (2017) 113–121.
- [35] A. Soria-Verdugo, L.M. Garcia-Gutierrez, S. Sanchez-Delgado, U. Ruiz-Rivas, Circulation of an object immersed in a bubbling fluidized bed, *Chem. Eng. Sci.* 66 (2011) 78–87.
- [36] A. Soria-Verdugo, L.M. Garcia-Gutierrez, N. García-Hernando, U. Ruiz-Rivas, Buoyancy effects on objects moving in a bubbling fluidized bed, *Chem. Eng. Sci.* 66 (2011) 2833–2841.
- [37] J.K. Sveen, MATPIV. <http://www.math.uio.no/jks/matpiv/>, 1998–2008.
- [38] L.A. Vandewalle, V. Francia, K.M. van Geem, G.B. Marin, M.O. Coppens, Solids lateral mixing and compartmentalization in dynamically structured gas–solid fluidized beds, *Chem. Eng. J.* 430 (4) (2022) 133063.
- [39] I.N.S. Winaya, T. Shimizu, D. Yamada, A new method to evaluate horizontal solid dispersion in a bubbling fluidized bed, *Powder Technol.* 178 (2007) 173–178.